Journal of the American Ceramic Society DOI: 10.1111/jace.14597 (2016)

Direct Visualization of Magnetic Field-Induced Magnetoelectric Switching in Multiferroic Aurivillius Phase Thin Films

Ahmad Faraz[1], Tuhin Maity[1], Michael Schmidt[1], Nitin Deepak[1], Saibal Roy[1], Martyn E. Pemble[1, 2], Roger W. Whatmore[2,3], Lynette Keeney[1i]

[1]Tyndall National Institute, University College Cork, 'Lee Maltings', Dyke Parade, Cork, Ireland

[2] Department of Chemistry, University College Cork, Cork, Ireland

[3]Department of Materials, Faculty of Engineering, Imperial College London, London, SW7 2AZ, United Kingdom

Multiferroic materials displaying coupled ferroelectric and ferromagnetic order parameters could provide a means for data storage whereby bits could be written electrically and read magnetically, or vice versa. Thin films of Aurivillius phase $Bi_6Ti_{2.8}Fe_{1.52}Mn_{0.68}O_{18}$, previously prepared by a chemical solution deposition (CSD) technique, are multiferroics demonstrating magnetoelectric coupling at room temperature. Here we demonstrate the growth of a similar composition, $Bi_6Ti_{2.99}Fe_{1.46}Mn_{0.55}O_{18}$, via the liquid injection chemical vapor deposition technique. High resolution magnetic measurements reveal a considerably higher in-plane ferromagnetic signature than CSD grown films (M_S = 24.25 emu/g (215 emu/cm^3), M_R = 9.916 emu/g (81.5 emu/cm^3), H_C = 170 Oe). A statistical analysis of the results from a thorough microstructural examination of the samples, allows us to conclude that the ferromagnetic signature can be attributed to the Aurivillius phase, with a confidence level of 99.95 %. In addition, we report the direct piezoresponse force

[i] E-mail: lynette.keeney@tyndall.ie

microscopy (PFM) visualization of ferroelectric switching while going through a full in-plane magnetic field cycle, where increased volumes (8.6 to 14 % compared with 4 to 7 % for the CSD-grown films) of the film engage in magnetoelectric coupling and demonstrate both irreversible and reversible magnetoelectric domain switching.

Introduction

Multiferroic materials which exhibit more than one mutually-coupled ferroic (e.g. ferroelectric (FE) / ferromagnetic (FM) / ferroelastic) order parameter (OP) in a single phase, provide additional degrees of OP freedom that can be exploited in novel multistate memory and sensing devices. Magnetoelectricity (the generation of a change in magnetization by an applied electric field or vice versa), on the other hand, is a related phenomenon that will arise in any material that is both electrically and magnetically polarizable and possesses an appropriate magnetic symmetry, regardless of whether it is multiferroic or not. For example, the magnetoelectric Cr_2O_3 is an antiferromagnetic dielectric and is neither FE nor FM[1]. The unique advantage of single phase magnetoelectric multiferroics is that not only could they find application in high storage density, low-power memory devices that can be electrically written and magnetically read, but also memory technologies with 4-state logic might be achieved by constructing devices that exploit the presence of both ferroelectric and ferromagnetic states[2] - representing a clear improvement over current 2-state logic devices. However, there are relatively few[3-8] materials demonstrating ferroelectric and ferromagnetic properties in a single-phase at room temperature. Due to conflicting electronic structure requirements for ferroelectricity (empty *d* orbitals) and ferromagnetism (partially filled *d* orbitals), the two properties tend to be mutually exclusive[9]. Examples of multiferroic materials which arise from lone-pair effects are the extensively studied[6, 7] room temperature ferroelectric (T_c 110

K)/antiferromagnetic (T_N 643 K) $BiFeO_3$ and doped derivatives[10, 11] (which also display a weak canted ferromagnetic moment) and $BiMnO_3$, which is a low temperature ferromagnetic oxide (T_c = ~105 K) reported to be ferroelectric (T_c = ~450 K) [12-14]. With improved materials design however, other structures showing multiferroic properties at ambient temperatures are now starting to emerge. For example, $(BiTi_{0.1}Fe_{0.8}Mg_{0.1}O_3)_{0.85}(CaTiO_3)_{0.15}$ is an example of a material system at a morphotropic phase boundary where ferroelectricity is enhanced and the magnetic ion concentration is above the percolation threshold for long-range magnetic order[5]. Another flexible layered system, $[Pb(Zr_{0.53}Ti_{0.47})O_3]_{0.6}$-$[Pb(Fe_{0.5}Ta_{0.5})O_3]_{0.4}$ (PZT-PFT), exhibits bilinear magnetoelectric coupling in lamellae of the ceramic at room temperature (~1 x 10^{-7} sm^{-1})[4] and magnetic fields of +3T can induce switching of ferroelectric domains that is comparable to that produced by electric fields (+25 V)[15].

By manipulating a family of layer-structured materials to accommodate both ferroelectric and ferromagnetic cations within the same structure, we previously synthesized Aurivillius phase $Bi_6Ti_{2.8}Fe_{1.52}Mn_{0.68}O_{18}$ by a chemical solution deposition (CSD) technique[3]. This material is a multiferroic thin film material that demonstrates a ferromagnetic signature (M_S = 0.74 emu/g, H_C = 7 Oe) and magnetoelectric coupling at room temperature. However, only 4 to 7 % of the films prepared by this CSD process engaged in magnetoelectric coupling. Furthermore, the relatively low remanent magnetization (M_R) value observed (M_R = 0.022 emu/g) restricts the use of these samples in potential memory device applications.

In this work, we demonstrate that thin films of $Bi_6Ti_{2.99}Fe_{1.46}Mn_{0.55}O_{18}$ (B6TFMO), grown by the industrially-compatible liquid injection chemical vapor deposition (LI-CVD) technique[16], produce a significantly stronger ferromagnetic signal (M_S of 24.25 emu/g) and increased volumes (8.6-14%) of the films engage in magnetoelectric coupling. Detailed microstructural analysis, coupled with a statistical analysis, allows us to conclude that the ferromagnetic signature does not

originate from minor magnetic impurity phases, with a confidence level of 99.95 %. In addition, we report the direct piezoresponse force microscopy (PFM) visualization of ferroelectric switching under the influence of a full in-plane magnetic field cycle and describe the effect of magnetic field on local ferroelectric hysteresis loops. Notably, both irreversible and reversible switching of ferroelectric domains by a magnetic field is observed. This work indicates the potential for B6TFMO thin films in future memory, sensing and actuating devices.

Experimental Procedure

Aurivillius phase $Bi_6Ti_{2.99}Fe_{1.46}Mn_{0.55}O_{18}$ (B6TFMO; *m* (the number of perovskite layers per half unit cell) = 5) thin films were grown via a liquid injection chemical vapor deposition (LI-CVD) technique[16] using the horizontal flow Aixtron AIX200/FE AVD (atomic vapor deposition) reactor equipped with an electronically controlled (µl/ms) liquid injection delivery system. Commercially available (SAFC-Hitech) liquid organometallic precursors $Bi(thd)_3$ (thd= 2,2,6,6-tetramethyl-3,5-heptanedionate), $Fe(thd)_3$, and $Ti(O\text{-}iPr)_2(thd)_2$ (O-iPr= iso-propoxide) dissolved in toluene were used for deposition at concentrations of 0.1 M. $Mn(thd)_3$ precursor solutions at a concentration of 0.025 M were prepared by dissolving $Mn(thd)_3$ (STREM Chemicals) in toluene under nitrogen in a glove box. These low vapor pressure precursors were injected into the Trijet Vaporizer of the LI-CVD system in and transferred onto 2" C-M plane (0001) oriented, 430 µm thick, single side polished sapphire substrates placed on a suscceptor rotated under a nitrogen flow at 60 rpm (to improve uniformity of deposition). 1:3 ratios of pure oxygen and nitrogen were used as oxidizing and precursor carrier gas (to the reaction chamber) for processing. The O_2 flow and processing deposition pressure were kept at 600 sccm (standard cubic centimeters per minute) and 10 mbar. The precursor volume ratios were kept at 7.5: 3: 1.5: 2 for $Bi(thd)_3$, $Ti(O\text{-}iPr)_2(thd)_2$, $Fe(thd)_3$ and $Mn(thd)_3$ respectively, which were controlled electronically by adjusting the pulse injection frequency and time

for the growth run. The net precursor flow is monitored by liquid flow meters (LFM). The vaporizer and substrate/reactor temperature were kept at 220 ºC and 610 ºC, respectively. Bismuth in excess (25 %) was used to avoid a deficiency of bismuth and to suppress the formation of secondary phases due to the volatile nature of bismuth at relatively high annealing temperatures (850 ºC for this sample), as is documented in the literature[3,17]. X-ray diffraction (XRD) profiles were collected using an X-pert PW3719 MPD diffractometer, equipped with a CuKα source (45KV and 40mA) and nickel (Ni) filter. The degree of crystallographic c-axis orientation, the Lotgering factor (L_f)[18, 19], was calculated by comparison of experimental diffracted line intensities with the theoretical values obtained using the Crystallographica software package[18]. Morphology and composition analysis were conducted using the FEI Helios Nanolab High-resolution scanning electron microscope (HR-SEM) and scanning transmission electron microscopy (STEM) modes and energy dispersive x-ray spectroscopy (EDX) equipped with an X-Max 80 detector and AZTec analysis software. A commercially available atomic force microscope (AFM MFP-3DTM; Asylum Research (AR)) in non-contact AC mode, equipped with silicon cantilevers (Olympus AC160TS) (Al reflective coating, 70 KHz electrilever resonance frequency and ~300-310 KHz contact resonance frequency), was used for surface roughness and topographical mapping. High resolution transmission electron microscopy (HR-TEM JEOL; 2100 TEM, 200 KV; double tilt holder) in conjunction with selected area electron diffraction (SAED) were used to perform microstructural analysis. Cross sections of B6TFMO films were prepared using a FEI Dual Beam Helios NanoLab 600i Focused Ion Beam (FIB) (final thinning at 93 pA, 30 kV, final polish 2 kV, 28 pA). Possible surface charging was prevented by gold coating. A superconducting quantum interference device (SQUID; Model-MPMS XL5, Quantum Design) magnetometer under maximum field of 5 T and 350 to 5 K temperature range was used for magnetic measurements. To ensure that there is no trapped flux both in the superconducting coil of SQUID and in the sample, a well-designed protocol was followed to demagnetize those[20]. The

superconducting coils of the SQUID are normally discharged from high field (5 T) to zero field in oscillation mode. The amount of trapped flux is typically <10 Oe for such cases. Before starting each new experiment, the superconducting coil was warmed to room temperature (350 K) which is above the critical point of the superconducting coil to remove any remanent magnetic field from the coil. Additionally, prior to any measurement, the sample itself was demagnetized with oscillating field using a well-designed demagnetizing protocol in order to ensure that there is no trapped flux in the sample. Local electromechanical measurements and visualization of ferroelectric domain emergence and switching under a magnetic field was performed by PFM (piezoresponse force microscopy) imaging equipped with a high voltage amplifier HVA220 (MFP-3D) under a magnetic field using the VFM2-HV (Asylum Research high voltage variable magnetic field module version 2). This system allows variable magnetic fields to be applied in-plane to the sample based on the rotation of a rare earth magnet. PFM images under cycled magnetic fields were collected at a scan angle 90 ^{o} and the magnetic field lines were parallel to the short axis of PFM electrilever (Olympus AC240TM Electrilevers, Ti/Pt-coated silicon cantilevers (Al reflex coated, 70 kHz resonant frequency, ~320 kHz contact resonance frequency) in the variable magnetic field imaging mode. The influence of the in-plane magnetic field on local in-plane ferroelectric domains were collected in the single frequency lateral PFM mode using an electrilever operating at a frequency (20 KHz) lower than the tip resonance (70 KHz) and tip/sample contact resonance frequency (300 to 310 KHz). Dual AC resonance switching spectroscopy PFM (DART-SS PFM), using a triangular step wave form of pulsed DC biases (15 V to 50 V), AC signal 5.5 V and cycling frequency (0.3 Hz) were used to generate local vertical piezoelectric hysteresis loops under the influence of the applied magnetic field. It should be noted that each of the newly used probes was calibrated and the optical lever sensitivity (InvOLs) of the probe was determined before generating hysteresis/strain loops according to the MFP-3D procedural manual.

Results

1000 injections of the above-described LI-CVD method produced B6TFMO samples of approximately 100 nm in thickness with rms roughness of 15 nm. XRD profiles (**Fig. 1(a)**) are consistent with an Aurivillius phase structure having 5 perovskite blocks per half unit cell (m = 5) with lattice parameters a = 5.38 Å, b = 5.43 Å, c = 50.26 Å. The samples are preferentially c-axis oriented with an L_f, of 0.998. XRD patterns are plotted with the intensities on a logarithmic scale ($\log_{10}$I) to highlight the minor or low intensity peaks and make them more visible[21]. HR-TEM (**Fig. 1(b)**) confirms the m = 5 layered Aurivillius structure, exhibiting some regions without out-of-phase boundaries (OPBs) (**Fig. 1b inset (i)**) and other regions with visible steps or OPBs (**Fig.1b inset (ii)**), typically seen for layered Aurivillius materials[22, 23]. Most (94 % approx.) of the perovskite-type layers were parallel to the sapphire substrate; however some (6 % approx.) were angled perpendicular to it (as analyzed over the scanned TEM areas). This is not inconsistent with the value of L_f, as the XRD was conducted in Bragg-Brentano geometry, which only samples crystal planes parallel to the substrate plane. OPBs frequently nucleate at the film-substrate interface due to a shift between regions of a crystal that are out-of-plane to the substrate and can propagate through the film. These regions are of the m = 5 layered B6TFMO structure, consistent with the parent phase. SEM-EDX measurements over a sample area of 25 x 25 μm^2 up to 1.2 x 1.2 mm^2, (analyzed by performing 5 scans on 5 different areas) demonstrate an average film composition of $Bi_6Ti_{2.99}Fe_{1.46}Mn_{0.55}O_{18}$.

Ferromagnetic hysteresis loops, (**Fig. 2(a)**), were observed for the sample throughout the temperature range (5 K to 300 K). The film porosity was taken into account for the magnetization calculations as we observed that an area of 0.16 % of the substrate was not covered by the B6TFMO film (**Fig.2a inset (i)**). The saturation magnetization (M_S = 24.25 emu/g or 215 emu/cm^3), coercive

field (H_C = 170 Oe) and remanence magnetization (M_R = 9.916 emu/g or 81.5 emu/cm^3) were calculated from these hysteresis curves at room temperature (300 K). Temperature dependent remanence magnetization (M_R) and coercivity (H_C) are plotted in **Fig.2b** where both the M_R and H_C gradually increase with decreasing temperature. Magnetization of B6TFMO as a function of temperature **(Fig.2b inset (i))** was investigated by field cooled (FC) and zero field-cooled (ZFC) curves respectively. A relatively low field of 100 Oe was applied for these measurements. From temperature dependent ZFC-FC measurements, the presence of magnetic phase transitions can be determined[20]. The clear split between the ZFC–FC curves below 350 K (**Fig.2b inset (i)**) and saturated hysteresis loops demonstrate the ferromagnetic nature of the material at room temperature and below, with T_c greater than 350 K, as otherwise the ZFC–FC lines would normally coincide with each other above T_c[24]. Hence both the field and temperature dependent measurements clearly demonstrate ferromagnetic behavior for the B6TFMO sample.

Direct local visualization of the magnetic-field-induced switching of ferroelectric domains via PFM was previously demonstrated for the CSD-grown $Bi_6Ti_{2.8}Fe_{1.52}Mn_{0.68}O_{18}$ thin films[3], where two distinct types of ferroelectric domain behavior were observed as the magnetic field was changed: (i) the emergence of in-plane piezoelectric domains and (ii) piezoelectric domain switching. In this work, we investigated the influence of a full magnetic field step cycle on the ferroelectric domains (**Fig. 3**). Ferroelectric domain nucleation and growth and local piezoelectric hysteresis (strain loops) were visualized using PFM[25-27] under in-plane variable magnetic fields (VFM). Aurivillius phase thin films are preferentially *c*-axis oriented with most of the grains having their crystallographic *a*-axis lying along the lateral plane of the film. The major polarization vector in these materials is along the in-plane *a*-axis[23]. Hence, this may result in larger in-plane ferroelectric polarizations coupling with the magnetic order parameters, compared to the out-of-plane polarization direction.

Single frequency lateral piezoresponse force microscopy[26] (SPFM ~20 KHz) under a variable magnetic field (0 Oe → +2500 Oe → 0 Oe → - 2500 Oe → 0 Oe) was used to explore local magnetic field induced in-plane ferroelectric domain switching in the B6TFMO thin films of thickness 100 nm and rms roughness of 15 nm (**Fig. 4** and **Fig. 5**).

Fig. 4(a-b) lateral amplitude and phase images demonstrate natural self-polarized piezoelectric domains at zero magnetic field (H) at room temperature. On increasing the magnetic field up to 1000 Oe (the field where nucleation begins) the emergence, nucleation and growth of magnetic field induced coupled ferroelectric domains were observed, these domains were not visible in the absence of applied external magnetic field (initial field of 0 Oe), as evident by an increase in response of the PFM amplitude and a 180 ° change in phase (see the contrast changes in the images, highlighted by the green circle in **Fig.4**). The lateral ferroelectric polarization was explored at a scan angle of 90 °, where motion along this axis is parallel to the magnetic field lines. As the torsional twist of the cantilever used for PFM scanning is parallel to the external applied VMF lines, the appearance, formation, and switching of newly formed ferroelectric domains are solely induced by the external magnetic field and a coupling of the electric and magnetic order parameters within the B6TFMO grains[14]. Domain growth was observed up to +2500 Oe (**Fig.4 (e-f)**) – this was the maxium magnetic field that was applied for these experiments. On reversal of the magnetic field direction back to 0 Oe **(Fig. 4 (i-j))**, it is evident that the piezoelectric domain persists and remains irreversible when cycled in the negative direction (**Fig.4 (m-n)**) and on completion of the magnetic field cycle (**Fig.4 (q-r)**).

Different types of magnetoelectric switching could be observed in the lateral PFM mode as demonstrated by regions of the sample circled in green and yellow in **Fig. 5**. On an increase in magnetic field from 0 Oe to +1000 Oe, a piezoelectric domain emerges in the region circled yellow

as demonstrated by an increase in piezoresponse (**Fig. 5 (c)**) and a change in phase contrast from purple to yellow (**Fig. 5 (d)**). The magnitude of the piezoresponse and the size of the piezoelectric domain increases on an increase in magnetic field to +2500 Oe (**Fig. 5 (e)** and **(f)**). On reversal of the magnetic field to +1500 Oe, the magnitude of the piezoresponse (**Fig. 5 (g)**) and the size of the piezoelectric domain decreases (**Fig. 5 (h)**) from that observed at +2500 Oe. On further reversal back to 0 Oe, the piezoelectric domain disappears, as evident by the region circled in yellow demonstrating no piezoresponse (**Fig. 5 (i)**) and a phase switch back to purple (**Fig. 5 (j)**), illustrating the reversibility of the magnetoelectric coupling under these conditions. On decreasing the magnetic field to -1500 Oe, the piezoelectric domain emerges again as demonstrated by an increase in piezoresponse (**Fig. 5 (k)**) and a change in phase contrast from purple to yellow (**Fig. 5 (l)**). The magnitude of the piezoresponse and the size of the piezoelectric domain increases on an increase in the strength of the negative magnetic field to -2500 Oe (**Fig. 5 (m)** and **(n)**), as was observed for the positive direction at +2500 Oe. On decrease in the magnetic field strength to -1500 Oe, the magnitude of the piezoresponse (**Fig. 5 (o)**) and the size of the piezoelectric domain decreases (**Fig. 5 (p)**) from that observed at +2500 Oe. On completion of the magnetic field cycle back to 0 Oe, the domain does not disappear, as demonstrated by a response in the amplitude image (**Fig. 5 (q)**) and a yellow phase contrast (**Fig. 5 (r)**), therefore, this magnetoelectric switching for this region is not fully reversible. A higher magnetic field of +2500 Oe is required to generate a piezoresponse (**Fig. 5 (e)**) and change in phase contrast (**Fig. 5 (f)**) for the region circled in green. This piezoelectric domain disappears on reversal of the magnetic field to +1500 Oe (**Fig. 5 (g)** and **(h)**) and is not observed on further decrease in magnetic field to 0G (**Fig. 4 (i)** and **(j)**) and to -1500 Oe (**Fig. 5 (k)** and **(l)**). However, the piezoelectric domain is generated on a decrease in magnetic field to -2500 Oe (**Fig. 5 (m)** and **(n)**), as was observed for the positive direction at +2500 Oe. This piezoelectric domain disappears on reversal of the magnetic field to -1500 Oe (**Fig. 5 (o)** and **(p)**) and is not observed on further decrease

in magnetic field to 0 Oe (**Fig. 5 (q)** and **(r)**). Upon the completion of the magnetic field cycle, it is evident that field dependent reversible magnetoelectric coupling behavior is observed for the region circled in green.

In order to investigate the influence of the magnetic field on vertical PFM domains, out-of-plane PFM measurements were performed on the B6TFMO thin films (of thickness 100 nm and rms roughness of 15 nm) using Dual AC resonance tracking PFM (DART-PFM), which is a mode designed to that amplify weak electromechanical signals along the vertical direction of B6TFMO thin films (by performing measurements at the tip sample contact resonance frequency ~300-310 KHz) while avoiding contributions from topographical crosstalk. The magnetic field induced ferroelectric polarization reversal behavior along the out-of-plane (vertical direction) is in good agreement with results obtained for the in-plane measurements. In parallel with the in-plane response, two different types of magnetoelectric coupled (i) irreversible (Type A) and (ii) reversible (Type B) switching was observed. The complete magnetic field cycle and magnetically induced amplitude and phase responses are illustrated in **Fig. 6 (a-t)**, using the magnetic field data points shown in **Fig. 3**. Vertical PFM amplitude and phase images in **Fig. 6 (a)** and **(b)**, respectively demonstrate that the LI-CVD-grown B6TFMO films are piezoelectric at room temperature at zero magnetic field. On increasing the magnetic field to 1000 Oe, two new piezoelectric domains emerge that were not observed at the initial field of 0 Oe, as evident by an increase in the PFM amplitude and a phase change to purple, highlighted by the green and yellow circles in **Fig. 6 (c)** and **(d)**. From +1000 Oe to +2500 Oe, the piezoelectric domains nucleate further, as is demonstrated by an increase in amplitude and size of the domains (**Fig. 6 (e)** and **(f)**). +2500 Oe was the maxium magnetic field that was applied for these experiments. When the magnetic field is reversed to +1500 Oe, the domain highlighted by the green circle demonstrates characteristics of Type A magnetoelectric coupling and

does not disappear, whereas the piezoelectric domain circled in yellow disappears, characteristic of grains that engage in Type B magnetoelectric switching. This grain does not demonstrate any piezoresponse at 0 Oe, however on further decrease in the negative direction to -1500 Oe, the piezoelectric domain emerges again and saturates at -2500G, as it did in the positive direction at +2500 Oe. On the other hand, the piezoelectric domain circled in green remains over the magnetic field cycle of +2500 Oe $\rightarrow$ 0 Oe $\rightarrow$ -2500 Oe. On completion of the magnetic field cycle back to 0 Oe (**Fig. 6 (q)** to **(r)**), the piezoresponse of the grain circled in yellow disappears, demonstrating reversible magnetoelectric switching, whereas the domain circled in green persists, demonstrating irreversible magnetoelectric switching. Note that AFM height (topography) images were collected simultaneously to the PFM imaging in **Figures 4**, **5** and **6** and no structural changes to the topography could be observed on cycling with the magnetic field.

The influence of the magnetic field on the piezoelectric response in B6TFMO was demonstrated by locally generating ferroelectric hysteresis loops on Type A and Type B domains (encircled in green and yellow, respectively in **Fig. 6 (a-t)**) as shown in **Fig. 7**. These loops were generated on removal of an applied DC-bias via DART switching spectroscopy PFM (DART-SSPFM[3, 26]. No PFM hysteresis loops were performed at ± 0 Oe. As is illustrated by the loops in **Fig. 7 (a)**, an increase in piezoresponse was observed on increasing the magnetic field from +1000 Oe to +2500 Oe for the Type A domain, which correlates with the increase in piezoresponse observed for the images in **Fig. 6 (c)** to **(e)**. No change in piezoresponse was observed for the loops generated on reversing the magnetic field to 0 Oe and on decreasing further to -1000 Oe and -2500 Oe, consistent with the piezoresponse images displayed in **Fig. 6 (e)** to **(m)**. The PFM hysteresis loops (**Fig. 7 (b)**) generated for the Type B domain demonstrates an increase in piezoresponse when increasing the magnetic field from +1000 Oe to +2500 Oe, consistent with what can observed for the region circled

in yellow in image **Fig. 6 (c)** to **(e)**. As was shown for the PFM images of the region circled in yellow (**Fig. 6 (e)** to **(m)**), the magnitude of the piezoresponse cycles with the magnetic field strength and direction: a decrease in piezoresponse is demonstrated for the PFM loops when the magnetic field is reversed to a negative field of -1000 Oe, which increases in magnitude when the strength of the negative magnetic field is increased to -2500 Oe.

Note that the PFM data describes magnetoelectric switching at the sample surface. It is not known whether magnetoelectric switching occurs through the thickness of the film also. The observed average switching regions in the B6TFMO thin films were a small fraction of the sample volume. The average magnetic field-induced in-plane polarization emergence was 14 % (**Fig. 4** and **Fig. 5**) and approx. 8.6 % for the out-of-plane vertical measurements (**Fig. 6**), although it must be noted that these percentage values are for distinct regions of the sample surface. However, increased volumes of the B6TFMO films grown by LI-CVD engage in magnetoelectric coupling compared with the CSD-grown films (4-7 % of the CSD-grown films engage in magnetoelectric coupling[3]. These results of direct magnetic field induced ferroelectric domain nucleation, growth and domain switching at the nanoscale within a single phase B6TFMO thin film are significant, and provide strong evidence for magnetoelectric switching behavior by providing direct visualization of magnetic field-controlled ferroelectric polarization. Hence, ferroelectric and ferromagnetic order parameters are correlated and coupled within a single phase B6TFMO at room temperature.

To confirm that the observed magnetoelectric multiferroic response was generated by the parent Aurivillius phase, detailed structural and compositional analysis is required to exclude the possible contribution of minor secondary phases to the observed ferromagnetic response, and a confidence level on that exclusion must be established. By performing a thorough microstructural phase analysis of the B6TFMO sample (refer to **Appendix**) and using a previously established

statistical model[28], we were able to calculate the upper bound volume fraction of unseen inclusions that would contribute to the remanent magnetization (M_R) of our B6TFMO sample. The details are outlined in the **Appendix**. We conclude that the observed ferromagnetism originates from the main B6TFMO Aurivillius phase to a confidence level of 99.95 %.

Discussion

The mechanism by which the magnetoelectric coupling and switching occurs in B6TFMO thin films is not obvious from these experiments. Evans *et al*. also report two types of magnetoelectric coupling behavior, bilinear PM (where *P* is polarization and *M* is magnetization) coupling and biquadratic (P^2M^2) coupling in $Pb(Zr,Ti)O_3$–$Pb(Fe,Ta)O_3$ ceramics, where the type of coupling is dependent on the magnetic field direction[29]. By considering highly generalized Landau free energy expressions and by monitoring the changes in capacitance that occur when a magnetic field is applied in each of three orthogonal directions, it was demonstrated that magnetocapacitance effects, consistent with P^2M^2 coupling, are strongest when fields are applied in the plane of the single crystal sheet investigated. Weaker P^2M^2 coupling was apparent when the magnetic field was perpendicular to the lamella where it was clear that asymmetric *PM* coupling terms were more dominant. It should be noted that detailed investigations on the influence of the crystallographic orientation of the B6TFMO grains with respect to the magnetic field on the nature of the magnetoelectric coupling are the subject of further work.

For our previously-reported CSD-derived $Bi_6Ti_{2.8}Fe_{1.52}Mn_{0.68}O_{18}$ thin films, SQUID magnetometry demonstrated values for M_S = 6.05 emu/cm^3, M_R = 0.18 emu/cm^3 and H_C = 70 Oe (at 300K)[3]. In this work, we report a significantly higher magnetic response for the LI-CVD-grown B6TFMO films at 300K of M_s = 215 emu/cm^3 or 24.25 emu/g (35 times higher than the CSD-grown films), M_R = 81.5 emu/cm^3 or 9.916 emu/g and Hc= 170 Oe. The magnetic data for the LI-CVD-

grown B6TFMO can be compared to Fe_2O_3 (M_R = 250 emu/cm^3 and M_S = 450 emu/cm^3)[30], commonly used in MRAM (magnetic random access memory)[31], and could be used in devices with potential applications in multistate logic and in-plane MRAM technologies.

It should be noted that M_R and H_C are extrinsic properties of the material, and depend on many physical factors such as roughness (rms roughness = 15 nm), texture, etc. The B6TFMO in this work prepared by the LI-CVD technique demonstrated structural homogeneity, as demonstrated by the fact that the majority of the sample is of the *m* = 5 structure, as shown by XRD and TEM. Additionally, B6TFMO films prepared by LI-CVD are denser (with porosity of 0.16 % compared with 2.44 % for the CSD-grown films).

Since compositional variation was noted for the previously-grown $Bi_6Ti_{2.8}Fe_{1.52}Mn_{0.68}O_{18}$ films[3], (the grain composition varied from Ti: Fe: Mn = 3.38: 1.14: 0.48 – 2.18: 2.16: 0.66)), elemental analysis was performed on individual Aurivillius phase grains of the LI-CVD-grown B6TFMO sample also to investigate whether there is grain-to-grain variation in magnetic ion content over the course of the sample. We selected 23 grains from a lamella of the B6TFMO thin film and performed elemental analysis, by STEM-EDX. EDX spectra across the 23 grains, followed by normalization of Ti: Fe: Mn ratios, shows a strong correlation between the Ti: Fe: Mn contents in these grains, with average ratio Ti (2.97): Fe (1.48): Mn (0.55) and composition $Bi_6Ti_{2.97}Fe_{1.48}Mn_{0.55}O_{18}$ (**Fig. 8a)**, similar to the average composition of the film ($Bi_6Ti_{2.99}Fe_{1.46}Mn_{0.55}O_{18}$) determined by SEM-EDX. The range of grain compositions varies from Ti: Fe: Mn = 2.85: 1.42: 0.45–3.15: 1.58: 0.59, demonstrating negligible compositional variation (**Fig. 8a)**. Therefore, the observation that only 8.6 to 14 % of the Aurivillius phase grains appear to engage in magnetoelectric coupling, as observed in the PFM investigations under a magnetic field (**Figures 4**, **5** and **6**), cannot be explained by compositional variation or increased levels of Fe/Mn in certain Aurivillius phase grains. This is in contrast to a relaxor ferroelectric perovskite system,

$(BiFe_{0.9}Co_{0.1}O_3)_{0.4}$–$(Bi_{1/2}K_{1/2}TiO_3)_{0.6}$ (BFC–BKT), that Henrichs et al.[32] describe. This system exhibits polar nanoregions which possess the ability to form congruent ferroelectric and ferrimagnetic regions, referred to as multiferroic clusters (MFC) within the perovskite matrix. Magnetoelectric coupling was observed via PFM and magnetic force microscopy within these MFC regions which were shown to originate from an increased local concentration of the $Bi(Fe,Co)O_3$ component.[32]

A previously proposed possible origin for the ferromagnetic behavior observed in $Bi_6Ti_{2.8}Fe_{1.52}Mn_{0.68}O_{18}$ CSD-derived thin films based on Goodenough–Kanamori (GEK) rules[3, 33] for quantum mechanical superexchange does not explain the increase in magnetization observed for the LI-CVD-grown films compared with the CSD-derived films. The GEK rule predicts ferromagnetic exchange when there is coupling between a magnetic cation with a filled orbital and a magnetic cation with a half-filled orbital. With a decrease in Ti^{4+} at the B-site of the perovskite (ABX_3) unit of the non-stoichiometric B6TFMO structure, to maintain chemical charge balance, it is possible that Mn exists in two different valance states, Mn^{4+} and Mn^{3+}. Mn^{4+} exhibits three un-paired electrons in its t_{2g} orbital and no electrons in the e_g orbitals in the perovskite coordination geometry, regardless of whether it is low-spin or high-spin. Hence, superexchange interactions are predicted to be ferromagnetic if there is an exchange between the electron in the e_g orbital of Fe^{3+} (d^5) and the empty e_g orbital in Mn^{4+} (d^3) , facilitated by the *p*-orbital of the oxygen anion within the perovskite unit cell[34]. However, the increased magnetic response observed for the B6TFMO films prepared in this work cannot be attributed to average differences in the Mn^{4+} content of the sample; the average composition of B6TFMO in this work is $Bi_6Ti_{2.99}Fe_{1.46}Mn_{0.55}O_{18}$, meaning that the average nominal content Mn^{4+} is 0.03 % (**Fig. 8b)**, compared with $Bi_6Ti_{2.8}Fe_{1.52}Mn_{0.68}O_{18}$ for the previously reported[3] CSD-derived samples, which has a nominal Mn^{4+} content of 0.6 %. However, the *B*-site location

and distribution of the Fe/Mn cations over the available sites within the perovskite-type layers within the Aurivillius phase unit cell may have consequences on the ferromagnetic response of the B6TFMO films and the extent of magnetoelectric coupling observed. Using first-principle calculations, Birenbaum *et al*. predicted a slight preference for the Fe^{3+} cation to occupy the "inner" sites within the perovskite-like layers of the *m=4* $Bi_5FeTi_3O_{15}$ system[35] and rather strong couplings of the order of $J_{NN} \sim 40–50$ meV for Fe^{3+} cations in nearest neighbor (NN) positions, characteristic of antiferromagnetic superexchange interactions. As explained above, NN superexchange interactions of Fe^{3+} and Mn^{4+} in B6TFMO would be expected to be ferromagnetic. However, the Fe^{3+} cations can also distribute in next-nearest-neighbor (NNN) positions at the inner *B*-sites, and the coupling between NNN is relatively weak ($J_{NNN} \sim 1–2$ meV) and becomes negligible among second-nearest neighbors. Although we do not presently have information on the *B*-site locations of the magnetic cations within the LI-CVD-grown $Bi_6Ti_{2.99}Fe_{1.46}Mn_{0.55}O_{18}$ or CSD-grown $Bi_6Ti_{2.8}Fe_{1.52}Mn_{0.68}O_{18}$ *m* = 5 systems, an increase in NN interactions leading to an increase in long-range magnetic order would give rise to increased magnetization values for the LI-CVD-grown $Bi_6Ti_{2.99}Fe_{1.46}Mn_{0.55}O_{18}$ sample.

Conclusions

In summary, we have produced m = 5 $Bi_6Ti_{2.99}Fe_{1.46}Mn_{0.55}O_{18}$ (B6TFMO) thin films via an industrially compatible LI-CVD process that displays optimized structural homogeneity and decreased porosity compared to the previously reported $Bi_6Ti_{2.8}Fe_{1.52}Mn_{0.68}O_{18}$ thin films prepared by CSD[3]. We report the first ever direct PFM visualization of the nucleation, growth and switching of ferroelectric domains under the influence of a full in-plane magnetic field cycle. Interestingly, two types of magnetoelectric coupling behavior were observed, (i) irreversible switching and (ii) reversible switching. The origin of the magnetoelectric coupling is not obvious from these

experiments. Crystallite orientation with respect to magnetic field direction may be a factor affecting the nature of the magnetoelectric coupling in the B6TFMO thin films. It is obvious from the TEM images (**Fig. 1 (b)**) and XRD data (**Fig. 1 (a)**), that the majority of the grains are oriented with their *a*-axes parallel to the substrate; however approximately 6 % of the sample has *a*-axis oriented grains which are tilted out-of-plane. Application of in-plane magnetic fields to the grains with their crystallographic *a*-axis lying in the lateral plane of the film may result in reversible Type B magnetoelectric switching, whereas it may result in irreversible Type A magnetoelectric switching for *a*-axis oriented grains which are tilted out-of-plane, however we can only speculate at this point. We observed significantly higher in-plane ferromagnetic signatures between 5K to 300K for the LI-CVD-grown $Bi_6Ti_{2.99}Fe_{1.46}Mn_{0.55}O_{18}$ samples as compared with the previous $Bi_6Ti_{2.8}Fe_{1.52}Mn_{0.68}O_{18}$ films grown by CSD[3]. The magnetic properties from these B6TFMO thin films, such as M_S = 24.25 emu/g (215 emu/cm^3), M_R = 9.916 emu/g (81.5 emu/cm^3) and Hc = 170 Oe are comparable to Fe_3O_4, used in MRAM applications[31]. We thoroughly scrutinized the B6TFMO films for the presence of trace levels of secondary phase magnetic impurities and conclude that the observed ferromagnetism originates from the main B6TFMO Aurivillius phase to a confidence level of 99.95 %. As such, we conclude that B6TFMO thin films can potentially be utilized for industrially compatible in-plane RAM applications and future high data storage multistate logic memory devices. More interestingly, demonstration of reversible ferroelectric switching by an external magnetic field is a very important finding as it allows the application of these films in magnetoelectric sensors and energy harvesters.

References

1. P. Borisov and W. Kleemann, Exchange bias and ferromagnetic coercivity in heterostructures with antiferromagnetic Cr2O3", *J. App. Phy*. **110** [3], 033917 (2011).

2. M. Gajek, M. Bibes, S. Fusil, K. Bouzehouane, J. Fontcuberta, A. Barthelemy and A. Fert, "Tunnel junctions with multiferroic barriers", *Nat. Mater*. **6** (4), 296-302 (2007).
3. L. Keeney, T. Maity, M. Schmidt, A. Amann, N. Deepak, N. Petkov, S. Roy, M. E. Pemble and R. W. Whatmore, "Magnetic Field-Induced Ferroelectric Switching in Multiferroic Aurivillius Phase Thin Films at Room Temperature", *J. Am. Ceram. Soc*., **96** [8] 2339–2357 (2013).
4. D. M. Evans, A. Schilling, A. Kumar, D. Sanchez, N. Ortega, M. Arredondo, R. S. Katiyar, J. M. Gregg, and J. F. Scott, "Magnetic switching of ferroelectric domains at room temperature in multiferroic PZTFT", *Nat. Comm*., **4**, 1534 (2013).
5. P. Mandal, M. J. Pitcher, J. Alaria, H. Niu, P. Borisov, P. Stamenov, J. B. Claridge and M. J. Rosseinsky, "Designing switchable polarization and magnetization at room temperature in an oxide", *Nature* **525**, 363-366 (2015).
6. R. Ramesh, "Magnetoelectrics: Making Metallic Memories," *Nat. Nanotech*., **5** [11] 761–2 (2010).
7. J. V. Dho, X. Qi, H. Kim, J. L. MacManus-Driscoll and M. G. Blamire, "Large electric polarization and exchange bias in multiferroic BiFeO3", *Adv. Mater*. **18**, 1445–1448 (2006).
8. M.-R. Li et al., "A Polar Corundum Oxide Displaying Weak Ferromagnetism at Room Temperature", *J. Am. Chem. Soc*., **134**, 3737 (2012).
9. N. A. Hill, "Why Are There so Few Magnetic Ferroelectrics?", *J. Phys. Chem. B.*, **104** (29), 6694-6709 (2000).
10. A. Mukherjee, S. Basu, P.K. Manna, S.M. Yusuf and M. Pal, "Enhancement of multiferroic properties of nanocrystalline BiFeO3 powder by Gd-doping", *J. Alloys Comp*., **598**, 142, (2014).

11. Ayan Mukherjee, Soumen Basu, P. K. Manna, S. M. Yusuf and Mrinal Pal, “Giant magnetodielectric and enhanced multiferroic properties of Sm doped bismuth ferrite nanoparticles”, J. Mater. Chem. C, **2**, 5885 (2014).
12. H. Chiba, T. Atou and Y. Syono, “Magnetic and electric properties of Bi1−xSrxMnO3: Hole-doping effect on ferromagnetic perovskite BiMnO3”, *J. Solid State Chem*., **132**, 139–143 (1997).
13. Y.-H. Chu, L. W. Martin, M. B. Holcomb, M. Gajek, S. J. Han, Q. He, N. Balke, C.-H. Yang, D. Lee, W. Hu, Q. Zhan, P.-L. Yang, A. Fraile-Rodriguez, A. Scholl, S. X. Wang, and R. Ramesh, “Electric-Field Control of Local Ferromagnetism Using a Magnetoelectric Multiferroic,” *Nat. Mat*., **7** [6] 478–82 (2008).
14. A. M. Mulders, “Multiferroics: Magnetic moments under stress”, *Nat. Phys*., **9**, 398–399 (2013).
15. D. M. Evans, A. Schilling, A. Kumar, D. Sanchez, N. Ortega, R. S. Katiyar, J. F. Scott and J. M. Gregg, “Switching ferroelectric domain configurations using both electric and magnetic fields in Pb(Zr,Ti)O3-Pb(Fe, Ta)O3 single-crystal lamellae,” *Phil. Trans. R. Soc. A*, **372**, 20120450 (2014).
16. M. Schumacher, P. K. Baumann and T. Seidel, “AVD and ALD as Two Complementary Technology Solutions for Next Generation Dielectric and Conductive Thin-Film Processing”, *Chem. Vap. Dep*., **12**, 99–108, (2006)).
17. L. Keeney, S. Kulkarni, N. Deepak, M. Schmidt, N. Petkov, P. F. Zhang, S. Cavill, S. Roy, M. E. Pemble and R. W. Whatmore, “Room Temperature Ferroelectric and Magnetic Investigations and Detailed Phase Analysis of Aurivillius Phase Bi5Ti3Fe0.7Co0.3O15 Thin Films” , *J. Appl. Phys*., **112** [5] 052010 (2012).
18. Crystallographica - a software toolkit for crystallography, Appl. Cryst 30, 418–419 (1997).

19. R. Furushima, S. Tanaka, Z. Kato and K.Uematsu, "Orientation distribution–Lotgering factor; relationship in a polycrystalline material—as an example of bismuth titanate prepared by a magnetic field", *Cer. Soc. Jpn*., **118** [10], 921-926 (2010).

20. T. Maity, S. Goswami, D. Bhattacharya and S. Roy, "Superspin Glass Mediated Giant Spontaneous Exchange Bias in a Nanocomposite of BiFeO3−Bi2Fe4O9", *Phys. Rev. Lett.*, **110** (10), 107201 (2013).

21. N. Deepak, P. F. Zhang, L. Keeney, M. E. Pemble and R. W. Whatmore, "*Atomic vapor deposition of bismuth titanate thin films*", *J. Appl. Phys*., **113**, 187207-187207 (2013).

22. M. A. Zurbuchen, W. Tian, X. Q. Pan, D. Fong, S. K. Streiffer, M. E. Hawley, J. Lettieri, Y. Jia, G. Asayama, S. J. Fulk, D. J. Comstock, S. Knapp, A. H. Karim and D. G. Schlom, "Morphology, structure and nucleation of out-of-phase boundaries (OPB) in epitaxial films of layered oxides", *J. Mater. Res*., **22** [6], 1439-1471 (2007).

23. R. E. Newnham, R. W. Wolfe and J. F. Dorrian, "Structural Basis of Ferroelectricity in the Bismuth Titanate Family", *Mat. Res. Bull*., **6**, 1029–1039 (1971).

J. Yang, L. H. Yin, Z. Liu, X. B. Zhu, W. H. Song, J. M. Dai, Z. R. Yang and Y. P. Sun, "Magnetic and dielectric properties of Aurivillius phase $Bi_6Fe_2Ti_3O_{18}$ and the doped compounds", *Appl. Phys. Lett*., **101**, 012402 (2012).

24. S. V. Kalinin, B. J. Rodriguez, S. Jesse, E. Karapetian, B. Mirman, E. A. Eliseev, and A. N. Morozovska, "Nanoscale Electromechanics of Ferroelectric and Biological Systems: A New Dimension in Scanning Probe Microscopy," *Ann. Rev. Mat. Res*., **37** [1] 189–238 (2007).

25. S. V. Kalinin, Z. G. Ye and A. L. Kholkin, "Preface to Special Topic: Piezoresponse Force Microscopy and Nanoscale Phenomena in Polar Materials", *J. Appl. Phys*., **112** [5] 051901 (2012).

26. S. V. Kalinin, N. Setter and A. L. Kholkin, “Electromechanics on the Nanometer Scale: Emerging Phenomena, Devices, and Applications,” *Mat. Res. Soc. Bull*., **34** [09] 634–42 (2009).

27. M. Schmidt, A. Amann, L. Keeney, M. E. Pemble, J. D. Holmes, N. Petkov and R. W. Whatmore, “Absence of Evidence ≠ Evidence of Absence: Statistical Analysis of Inclusions in Multiferroic Thin Films”, *Sci. Rep*., **4**,5712 (2014).

28. D. M. Evans, A. Schilling, A. Kumar, D. Sanchez, N. Ortega, R. S. Katiyar, J. F. Scott and J. M. Gregg, “The Nature of Magnetoelectric Coupling in Pb(Zr,Ti)O3–Pb(Fe,Ta)O3”, *Adv. Mat*., **27**, 6068-6073 (2015).

29. J. Mizusaki, N. Mori, H. Takai, Y. Yonemura, H. Minamiue, H. Tagawa, M. Dokiya, H. Inaba, K. Naraya, T. Sasamoto and T. Hashimoto, “Oxygen Nonstoichiometry and Defect Equilibrium in the Perovskite Type Oxides La1-xSrxMnO3+d”, *Sol. State Ion*., **129** [1–4] 163–77 (2000).

30. K. Kukli, M. C. Dimri, A. Tamm, M. Kemell, T. Käämbre, M. Vehkamäki, M. Puttaswamy, R. Sternc, I. Kuusik, A. Kikas, M. Tallarida, D. Schmeißer, M. Ritala and M. Leskeläa, “Structural and Magnetic Studies on Iron Oxide and Iron-Magnesium Oxide Thin Films Deposited Using Ferrocene and (Dimethylaminomethyl) ferrocene Precursors”, *ECS J. Solid State Sci. Technol.*, **2**, N45-N54 (2013).

31. L. F. Henrichs, O. Cespedes, J. Bennett, J. Landers, S. Salamon, C. Heuser, T. Hansen, T. Helbig, O. Gutfleisch, D. C. Lupascu, H. Wende, W. Kleemann and A. J. Bell, ‘Multiferroic Clusters: A New Perspective for Relaxor-Type Room-Temperature Multiferroics’, *Adv. Funct. Mater*., **26**, 2111–2121 (2016),

32. J. B. Goodenough, “Theory of the Role of Covalence in the Perovskite Type Manganites [La, M(II)]MnO3,” *Phys. Rev*., **100** [2] 564–73 (1955).

33. Y. Zhou, X. Jin and I. V. Shvets, “Enhancement of the magnetization saturation in magnetite (100) epitaxial films by thermo-chemical treatment”, *J. App. Phys*., **95** [11], (2004).

34. A. Y. Birenbaum and C. Ederer, "The potentially multiferroic Aurivillius phase Bi5FeTi3O15: cation site preference, electric polarization, and magnetic coupling from first-principles", *Phys. Rev. B.*, **90**, 214109 (2014).

Acknowledgments: The support of the 7th Framework Programme Marie Curie Initial Training Network under the NANOMOTION Grant agreement no.: 290158 is gratefully acknowledged. This publication has emanated from research conducted with the financial support of the Royal Society and Science Foundation Ireland (SFI) University Research Fellowship UF 140263 and SFI under Grant "SFI 13/TIDA/I2728''. The support of SFI under the FORME Strategic Research Cluster Award number 07/SRC/I1172 and the Irish Higher Education Authority (HEA) PRTLI 3, HEA PRTLI4 and Project INSPIRE is gratefully acknowledged.

List of Figures

Fig.1 (a) XRD pattern over the scan range $5 \leq 2\Theta \leq 37.5°$ illustrating the c-axis oriented ($L_f \approx 0.998$) single phase m = 5 Aurivillius $Bi_6Ti_{2.99}Fe_{1.46}Mn_{0.55}O_{18}$ phase thin film grown on <001> oriented sapphire substrate. The asterisks indicate substrate peaks. **(b)** A representative cross-section HRTEM image confirming a uniform m = 5 layered Aurivillius phase structure. Inset **(i)** m=5 is representative of the majority of the sample without out-of-phase boundaries (OPBs) and inset **(ii)** is illustrative of regions (6% appx.) with visible OPBs.

Fig.2 (a) Magnetization (M; emu/g) versus magnetic field (H; Oe) for the $Bi_6Ti_{2.99}Fe_{1.46}Mn_{0.55}O_{18}$ sample. Inset image **(i)** in (a) displays an SEM image of the sample illustrating the presence of 0.16

% pores (yellow arrows). **(b)** Magnetic parameters M_R (remanence magnetization) and H_C (coercive field) versus versus T (K) (temperature) for the $Bi_6Ti_{2.99}Fe_{1.46}Mn_{0.55}O_{18}$ sample. Inset image **(i)** zero field cooled (ZFC) and field cooled (FC) measurements (M_R versus T (K)).

Fig.3 Representation of the full magnetic field step cycles of the magnetic field applied to the ferroelectric films. The letters indicate the fields at which the corresponding images were taken in Figures 4, 5 and 6.

Fig.4 (**a** - **r**) Representative images of the effect of a complete magnetic field cycle (0 Oe $\rightarrow$ +2500 Oe $\rightarrow$ 0 Oe $\rightarrow$ -2500 Oe$\rightarrow$ 0 Oe) applied locally to the $Bi_6Ti_{2.99}Fe_{1.46}Mn_{0.55}O_{18}$ thin film sample on the in-situ in-plane (lateral) piezoresponse force microscopy measurements. **(s)** topography, **(t)** scale key for phase contrast, **(u) s**cale key for sample area, **(v)** scale key for topography contrast. The images demonstrate magnetic field induced irreversible (Type A) ferroelectric domain nucleation **(a,b)**, growth **(c,d)**, saturation **(e,f)** and irreversible switching under the magnetic field cycle.

Fig.5 (**a** - **r**) Representative images of the effect of a complete magnetic field cycle (0 Oe $\rightarrow$ +2500 Oe $\rightarrow$ 0 Oe $\rightarrow$ -2500 Oe$\rightarrow$ 0 Oe) applied locally to the $Bi_6Ti_{2.99}Fe_{1.46}Mn_{0.55}O_{18}$ thin film sample on the in-situ in-plane (lateral) piezoresponse force microscopy measurements. **(s)** topography, **(t)** scale key for phase contrast, **(u) s**cale key for sample area, **(v)** scale key for topography contrast. The images demonstrate magnetic field induced reversible (Type B) ferroelectric domain nucleation **(a,b)**, growth **(c,d)**, saturation **(e,f)** and reversible switching under the magnetic field cycle for the area encircled green and partially reversible switching for the area encircled yellow.

Fig.6 (**a** - **r**) Representative images of the effect of a complete magnetic field cycle (0 Oe → +2500 Oe → 0 Oe → -2500 Oe→ 0 Oe) applied locally to the $Bi_6Ti_{2.99}Fe_{1.46}Mn_{0.55}O_{18}$ thin film sample on the in-situ out-of-plane (vertical) piezoresponse force microscopy measurements. **(s)** topography, **(t)** scale key for phase contrast, **(u) s**cale key for sample area, **(v)** scale key for topography contrast. The images demonstrate magnetic field induced irreversible (encircled green) (Type A) and reversible (encircled yellow) (Type B) ferroelectric domain nucleation **(a,b)**, growth **(c,d)**, saturation **(e,f)** under the magnetic field cycle.

Fig.7. The effect of applied magnetic field on the PFM strain loops generated from the $Bi_6Ti_{2.99}Fe_{1.46}Mn_{0.55}O_{18}$ thin film sample. (a) an irreversibly-coupled domain (Type A) shown in Inset image (i) encircled green and (b) a reversibly-coupled domain (Type B) shown in Inset image (i) encircled yellow.

Fig.8 (a) Plot of the normalized B-site composition of Fe and Mn vs that for Ti, as determined by cross-section HR-STEM-EDX from 23 Aurivillius grains within the $Bi_6Ti_{2.99}Fe_{1.46}Mn_{0.55}O_{18}$ sample. (**b)** Plot of the total B-site Mn composition and B-site Mn^{4+} composition, calculated to maintain charge balance, vs the B-site Fe composition.

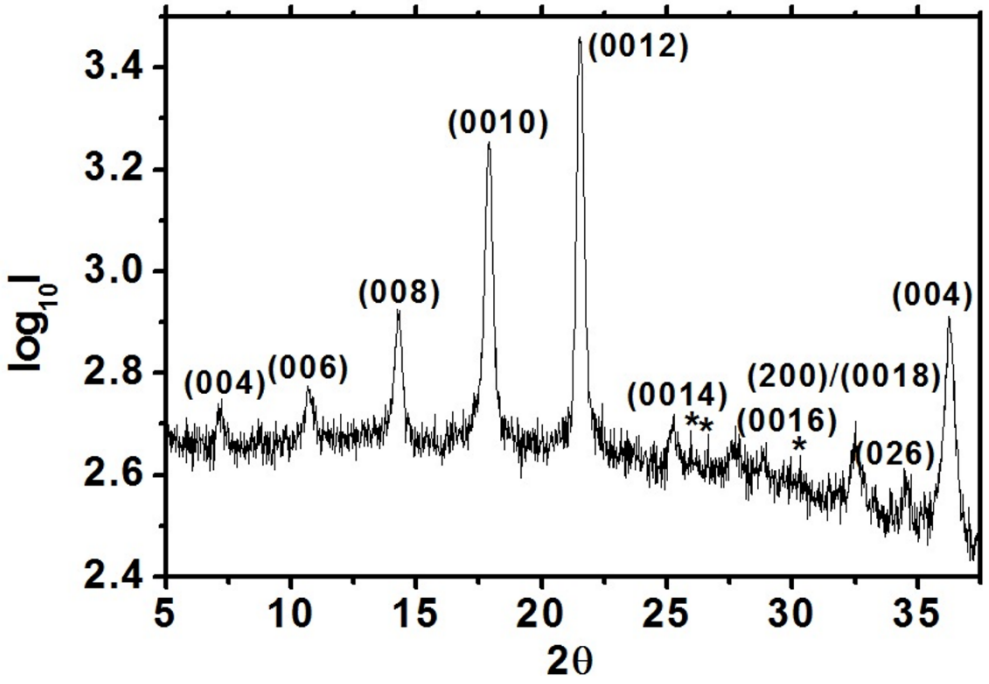
log10 I
2θ
(004)
(006)
(008)
(0010)
(0012)
(0014)
**
(0016)
*
(200)/(0018)
(026)
(004)
3.4
3.2
3.0
2.8
2.6
2.4
5
10
15
20
25
30
35

Figure 1a

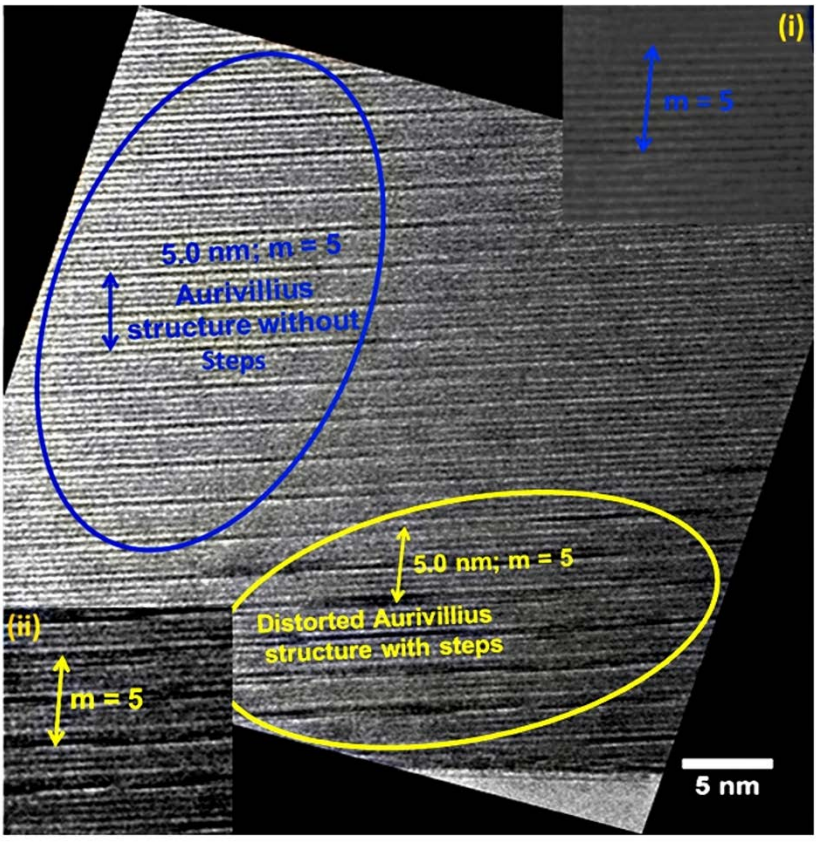
(i)
m = 5
5.0 nm; m = 5
Aurivillius
structure without
Steps
5.0 nm; m = 5
Distorted Aurivillius
structure with steps
(ii)
m = 5
5 nm

Figure 1b

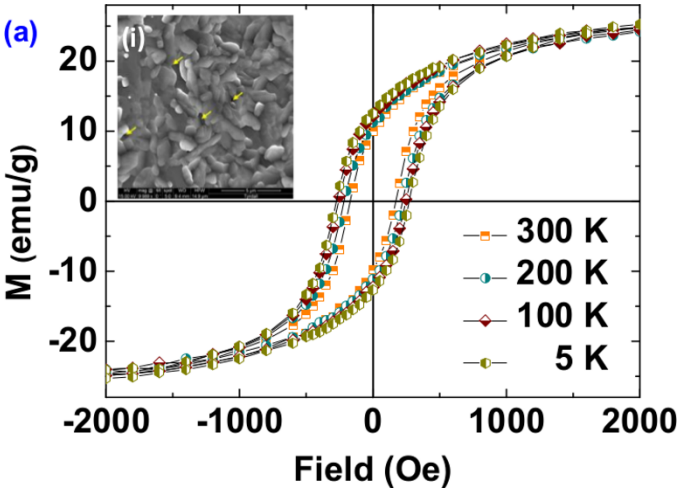

Figure 2a

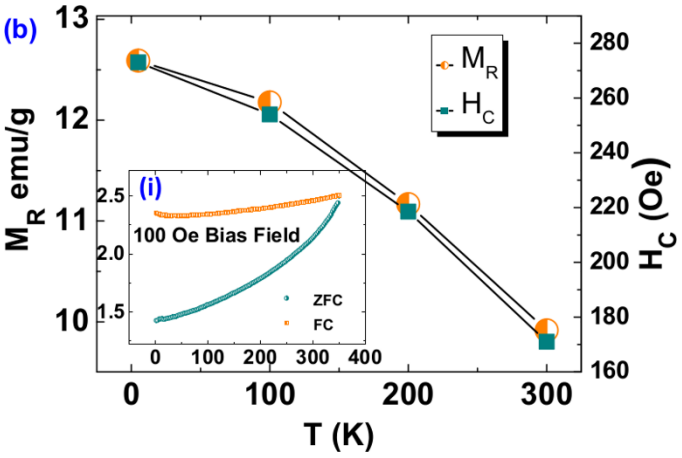

Figure 2b

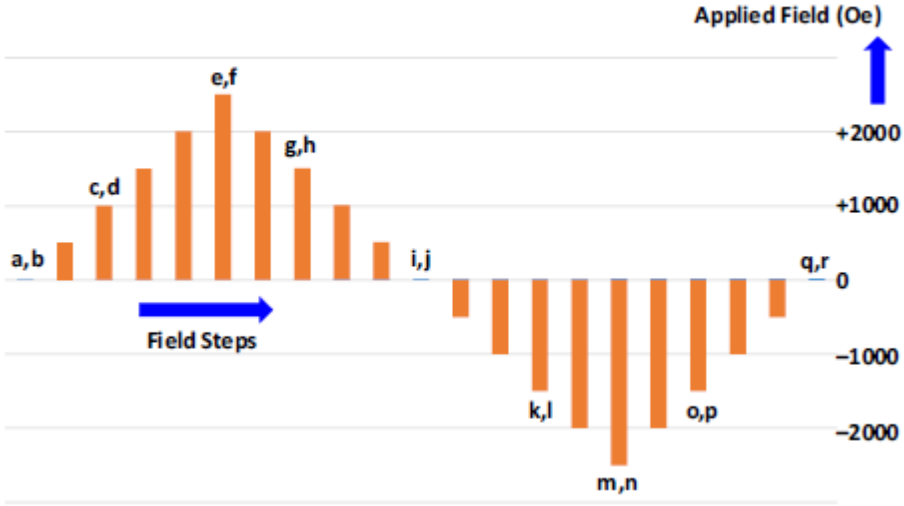

Figure 3

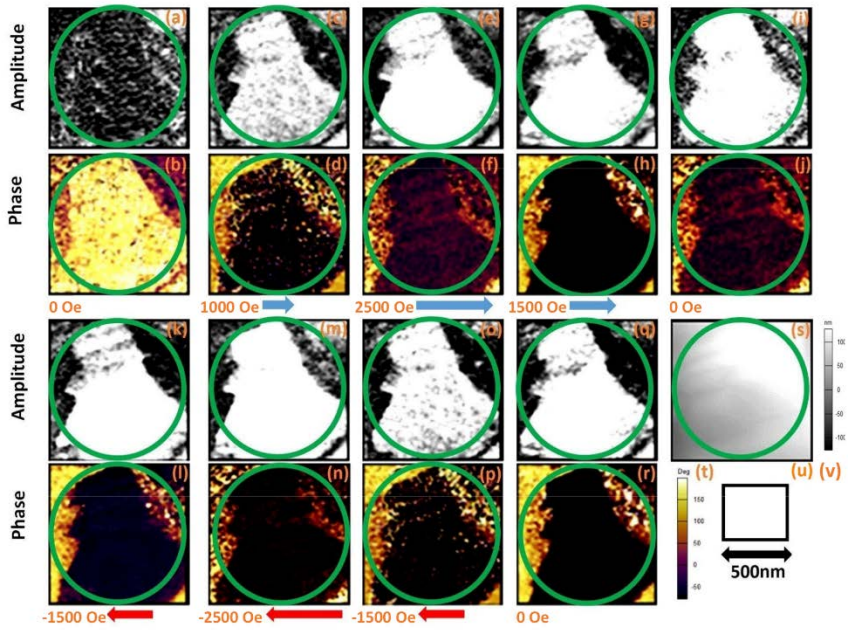

Figure 4

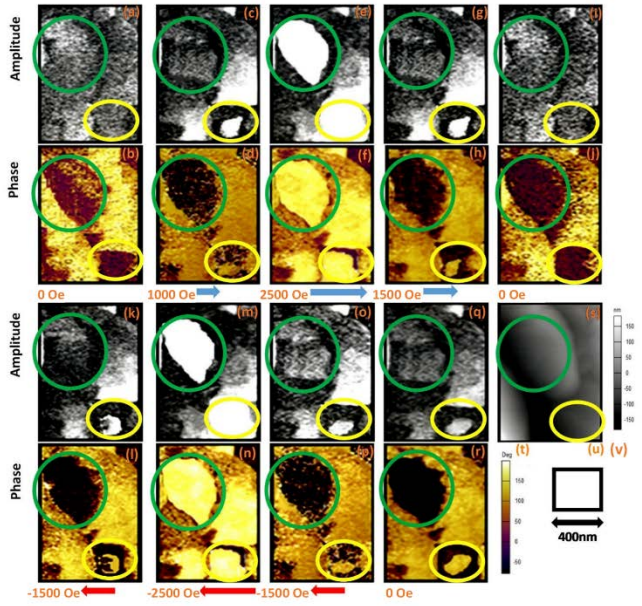

Figure 5

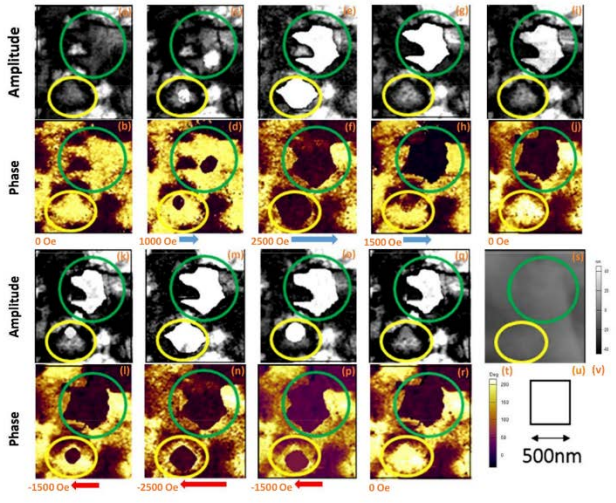

Figure 6

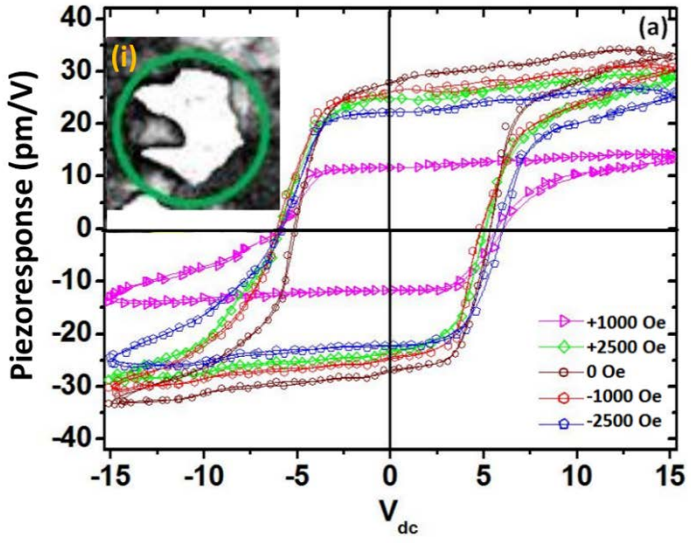

Figure 7a

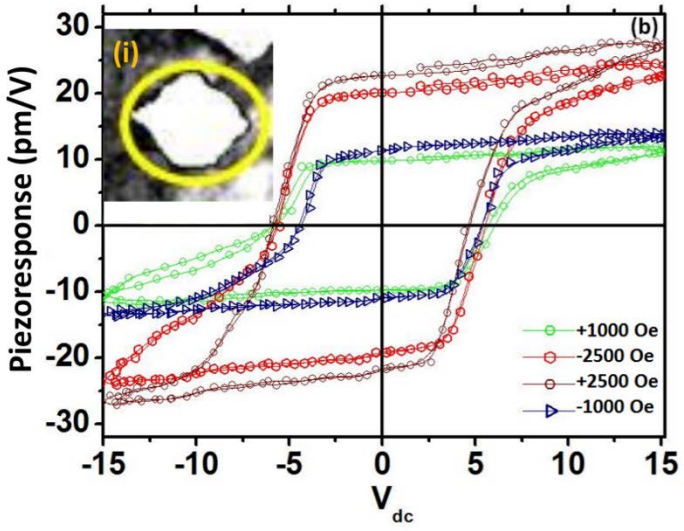

Figure 7b

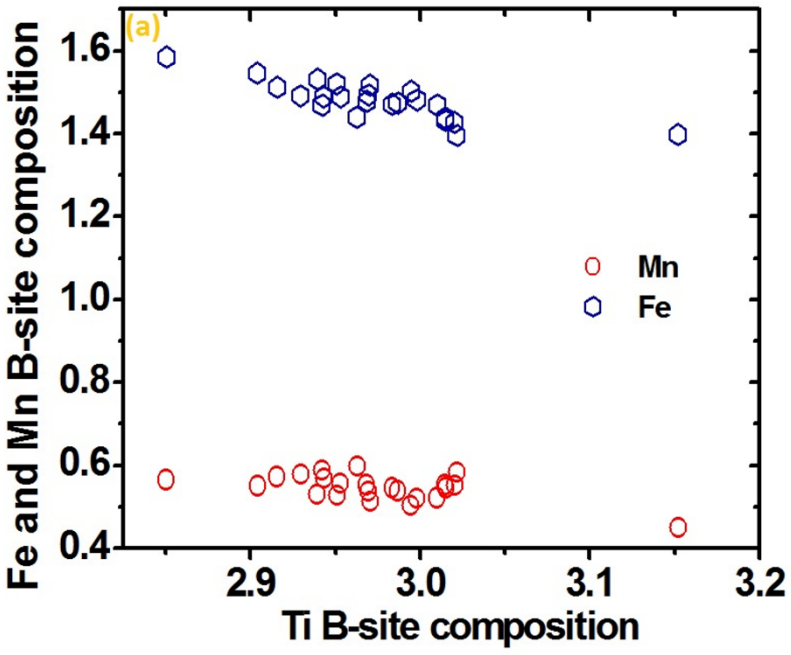

Figure 8a

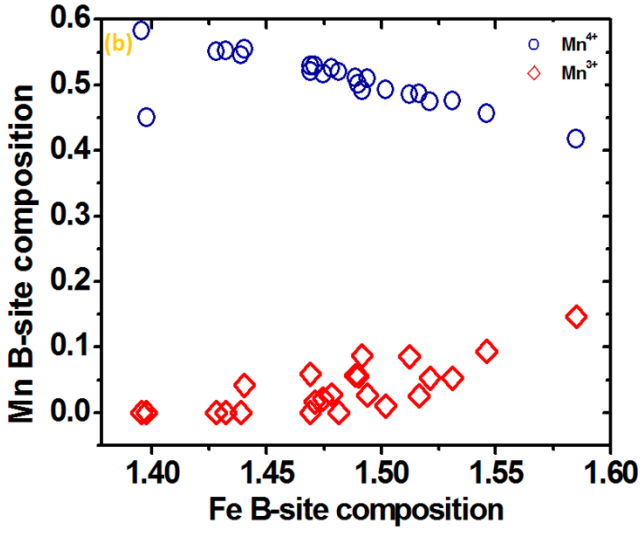

Figure 8b

Journal of the American Ceramic Society DOI: 10.1111/jace.14597 (2016)

Direct Visualization of Magnetic Field-Induced Magnetoelectric Switching in Multiferroic Aurivillius Phase Thin Films

Ahmad Faraz[1], Tuhin Maity[1], Michael Schmidt[1], Nitin Deepak[1], Saibal Roy[1], Martyn E. Pemble[1, 2], Roger W. Whatmore[2,3], Lynette Keeney[1ii]

[1]Tyndall National Institute, University College Cork, 'Lee Maltings', Dyke Parade, Cork, Ireland

[2] Department of Chemistry, University College Cork, Cork, Ireland

[3]Department of Materials, Faculty of Engineering, Imperial College London, London, SW7 2AZ, United Kingdom

Appendix

Particular care was taken to assess the possibility of the presence of ferroelectric (frustrated pyrochlore/ intergrowth etc.) [1, 2] and/or ferromagnetic (spinel)[3] minor secondary phases; as such phases might confuse the unequivocal detection of ferroelectric and ferromagnetic signatures. No reflections indicative of possible minor impurities such as the pyrochlore (prominent (444) reflection expected at 29.96 °) and spinel structures (prominent (311) reflection is expected at 35.4 °) over the XRD scan range 5 ° ≤ 2Θ ≤ 37.5° were observed (**Fig. 1 (a)**). The presence of possible spinel impurities were investigated further using XRD with a slower x-ray scan rate of 0.25 °/min and a step size of 0.005 ° (**Appendix Fig. 1**), performed in the range 34.5 ° ≤ 2Θ ≤ 36.5 °. However, the background noise level during XRD scanning limits the detectability of minor phases and trace levels below 3 vol% of the parent composition are typically undetectable. Yet if present, they may affect the overall magnetization of the sample[4]. In such situations, composition, morphology and thorough

[ii] E-mail: lynette.keeney@tyndall.ie

structural analysis is required[5] to confirm that the material in question is a genuine single phase multiferroic, with the ferroelectric and ferromagnetic properties originating from the parent phase. HR-SEM-EDX surface scans over a 72 hr time period on a sample area of (1.2 x 1.2 mm^2) were performed to analyze the sample morphology and composition to assess the volume of any magnetic inclusions visible. A 72 hr HR-SEM-EDX scan, followed by subtraction of BiLα from FeKα signals demonstrates the presence of three Fe-rich inclusions in the diameter range of 1 to 3 μm which are labelled as A, B and C in **Appendix Fig. 2**, **3 and 4**. HR-TEM/SAED (**Fig. 2 (a-c) and Fig. 3(a-c)**) demonstrates that the inclusions A and B closely correspond to a $BiFeO_3$ perovskite-type structure exhibiting d-spacings of 5.7 Å and 5.6 Å, respectively. Inclusion C (**Appendix Fig. 4)** demonstrates a similar crystal shape to inclusions A and B and the EDX data corresponds to the perovskite $BiFeO_3$, however, inclusion C was amorphosized and over thinned during FIB sample preparation, therefore no cross section TEM data could be obtained. These non-magnetic $BiFeO_3$ perovskite-type inclusions, present in the B6TFMO sample at a volume fraction of 0.006 % do not contribute to the magnetic response observed for the B6TFMO sample. In addition, although $BiFeO_3$ is a known room temperature magnetoelectric, the presence of this type of inclusion at this minor volume fraction would not account for magnetoelectric switching in B6TFMO given that the percentage of the B6TFMO sample observed to engage in magnetoelectric switching is >8 %. No magnetic impurity phases were detected by EDX analysis of the 1.2 x 1.2 mm^2 area of the B6TFMO sample over the 72 hr time period.

We effectively improved the signal to noise ratio (SNR) and investigated the presence of impurity phases having an effect on the remanence polarization (M_R) down to 0.01 vol%, by performing a number of measurements, and for each measurement, the scanned volume and the minimal detectable inclusion size was recorded, in a similar manner to that illustrated by Schmidt *et al*.[5], as completely

summarized in **Table 1**. Conclusive remarks on the vol% of magnetic inclusions and their effect on magnetic response was established by using a statistical model considering the worst case scenario for unseen embedded inclusions which enables us to calculate the upper bound contribution that undetected magnetic inclusions would have on the remanent magnetization (M_R) of the B6TFMO sample. Since no magnetic inclusions were detected, we assume a worst case scenario that the magnetic properties of any undetected inclusions are comparable with the candidate Fe_3O_4, which has the strongest known M_R for consideration as an impurity phase in these Aurivillius-phase systems. We assume that inclusions with diameter <5 nm are not ferromagnetic and would not contribute to the observed magnetic response. Inclusions with diameters between 5-20nm have M_R of 10 emu/g[3] and all the other inclusions have an M_R of 20 emu/g, comparable with bulk Fe_3O_4[6]. These upper estimates were used to calculate the contribution that unseen inclusions of this type would have on the M_R value of our B6TFMO sample. This is performed in the column denoted by $M_{R,k}$ in **Table 1**. The maximum $M_{R,k}$ value is 0.371 *m*emu/g. From these statistical calculations, the contribution of undetectable inclusions below the size range of 5 nm is <0.371 *m*emu/g (0.004% of net M_R = 9.916 emu/g) with a confidence level better than 99.95 %. Hence, we conclude the effect of undetected inclusions/secondary phases on the magnetic or magnetoelectric properties of B6TFMO is negligible.

References

1. P. F. Zhang, N. Deepak, L. Keeney, M. E. Pemble and R. W. Whatmore, “The structural and piezoresponse properties of c-axis-oriented Aurivillius phase Bi5Ti3FeO15 thin films deposited by atomic vapor deposition,” *Appl. Phys. Lett.*, **101**, 112903-112904 (2012).
2. R. Seshadri, “Lone pairs in insulating pyrochlores: Ice rules and high-k behavior”, *Sol. State Sci.*, **8**, 259-66, (2006).

3. L. Keeney, T. Maity, M. Schmidt, A. Amann, N. Deepak, N. Petkov, S. Roy, M. E. Pemble and R. W. Whatmore, "Magnetic Field-Induced Ferroelectric Switching in Multiferroic Aurivillius Phase Thin Films at Room Temperature", *J. Am. Ceram. Soc.*, **96** [8] 2339–2357 (2013).
4. L. Keeney, S. Kulkarni, N. Deepak, M. Schmidt, N. Petkov, P. F. Zhang, S. Cavill, S. Roy, M. E. Pemble and R. W. Whatmore, "Room Temperature Ferroelectric and Magnetic Investigations and Detailed Phase Analysis of Aurivillius Phase Bi5Ti3Fe0.7Co0.3O15 Thin Films", *J. Appl. Phys.*, **112** [5] 052010 (2012).
5. M. Schmidt, A. Amann, L. Keeney, M. E. Pemble, J. D. Holmes, N. Petkov, R. W. Whatmore, "Absence of Evidence ≠ Evidence of Absence: Statistical Analysis of Inclusions in Multiferroic Thin Films", Sci. Rep., **4**,5712 (2014).
6. N. N. Guan, Y. T. Wang, D. J. Sun, and J. Xu, "A Simple One-Pot Synthesis of Single-Crystalline Magnetite Hollow Spheres from a Single Iron Precursor", Nanotechnology, **20** [10] 105603 (2009).

Acknowledgments: The support of the 7th Framework Programme Marie Curie Initial Training Network under the NANOMOTION Grant agreement no.: 290158 is gratefully acknowledged. This publication has emanated from research conducted with the financial support of the Royal Society and Science Foundation Ireland (SFI) University Research Fellowship UF 140263 and SFI under Grant "SFI 13/TIDA/I2728''. The support of SFI under the FORME Strategic Research Cluster Award number 07/SRC/I1172 and the Irish Higher Education Authority (HEA) PRTLI 3, HEA PRTLI4 and Project INSPIRE is gratefully acknowledged.

List of Appendix Figures:

Appendix Fig.1 Representative XRD pattern, taken at a slower scan rate of 0.25°/min and a step size of 0.005°performed in range $34.5 \leq 2\Theta \leq 36.5°$.

Appendix Fig.2 (a) HR-SEM-EDX surface scans over a 72 hr time period on a sample area of (1.2 x 1.2 mm^2) demonstrating the morphology of inclusion A. (b) HRTEM for inclusion A demonstrating d-spacing of 5.7 Å. (c) SAED for inclusion A.

Appendix Fig.3 (a) HR-SEM-EDX surface scans over a 72 hr time period on a sample area of (1.2 x 1.2 mm^2) demonstrating the morphology of inclusion B. (b) HRTEM for inclusion B demonstrating d-spacings of 5.6 Å. (c) SAED for inclusion B.

Appendix Fig.4 HR-SEM-EDX surface scans over a 72 hr time period on a sample area of (1.2 x 1.2 mm^2) (a-b) SEM images demonstrating morphology of Inclusion C. This inclusion was subsequently over-thinned during FIB preparation, hence no information could be gained via cross section TEM.

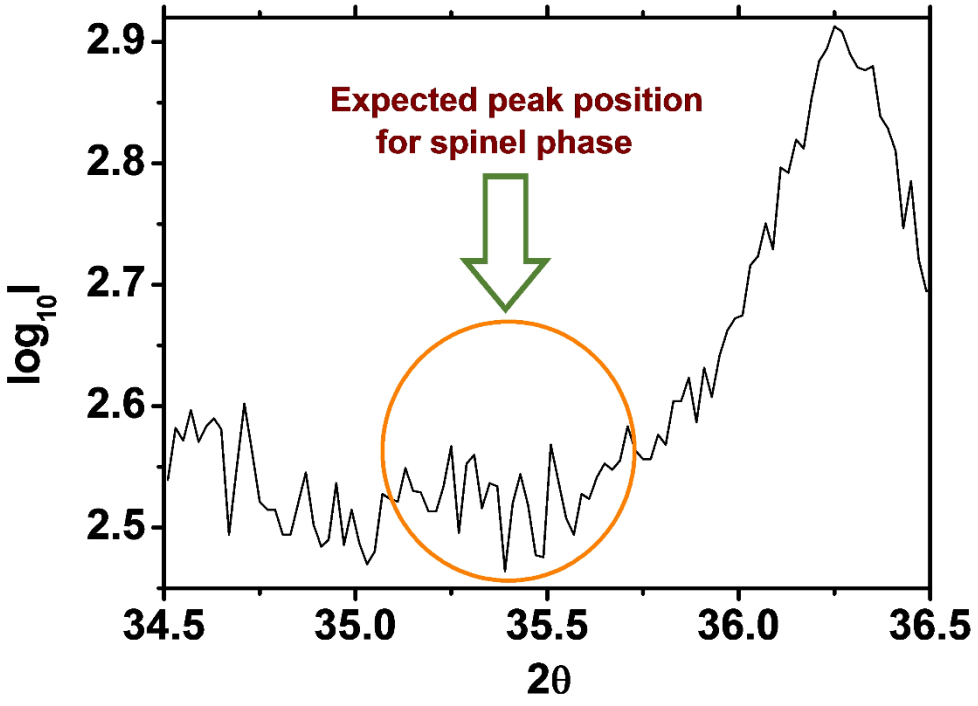

Appendix Figure 1

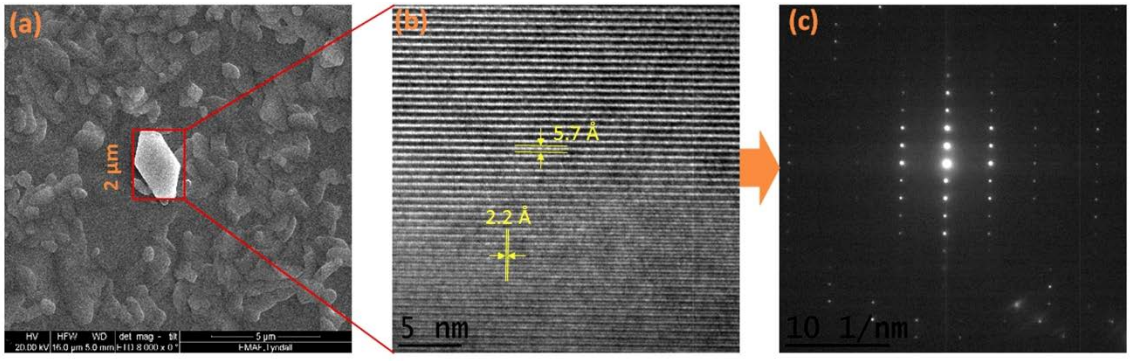

Appendix Figure 2

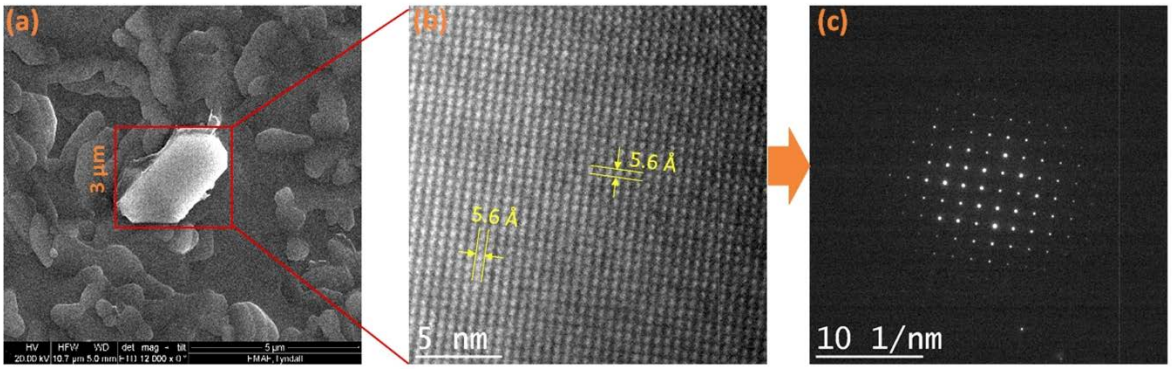

Appendix Figure 3

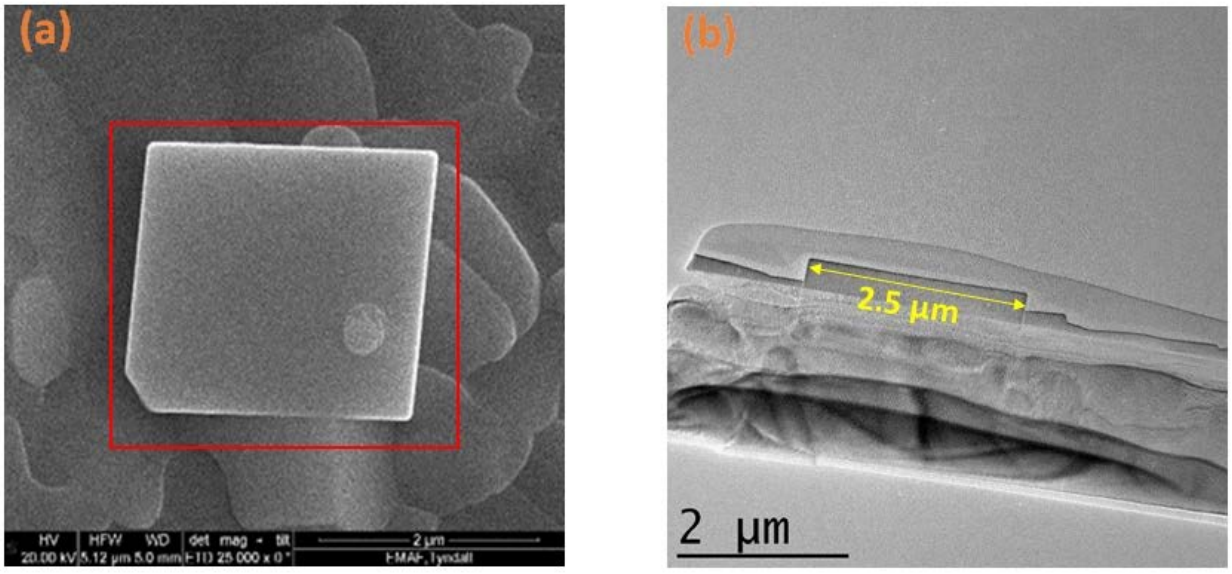

Appendix Figure 4